

## Pressure coefficients of Raman modes of carbon nanotubes resolved by chirality: Environmental effect on graphene sheet

A. J. Ghandour,<sup>1,2</sup> I. F. Crowe,<sup>3</sup> J. E. Proctor,<sup>4</sup> Y. W. Sun,<sup>1</sup> M. P. Halsall,<sup>3</sup> I. Hernandez,<sup>1,5</sup> A. Sapelkin,<sup>1</sup> and D. J. Dunstan<sup>1,\*</sup>

<sup>1</sup>*School of Physics and Astronomy, Queen Mary University of London, London E1 4NS, UK*

<sup>2</sup>*Department of Physics, Faculty of Sciences 5, Lebanese University, Nabatieh, Lebanon*

<sup>3</sup>*Photon Sciences Institute and School of Electrical and Electronic Engineering, University of Manchester, Manchester M13 9PL, UK*

<sup>4</sup>*Department of Physics, University of Hull, Hull HU6 7RX, UK*

<sup>5</sup>*MALTA Consolider Team, Departamento CITIMAC, Facultad de Ciencias, Universidad de Cantabria, 39005 Santander, Spain*

(Received 10 May 2012; revised manuscript received 14 December 2012; published 13 February 2013)

Studies of the mechanical properties of single-walled carbon nanotubes are hindered by their availability only as ensembles of tubes with a range of diameters. However, tunable Raman spectroscopy is capable of identifying individual tubes from such ensembles. Interestingly, both the radial breathing mode and, surprisingly, the  $G$ -mode pressure coefficients exhibit strong environmental effects, which are largely independent of the nature of the environment. We show that the  $G$ -mode pressure coefficient varies with diameter, consistent with the thick-wall tube model. Reappraisal of literature data for graphene and graphite suggests revision of both the  $G$ -mode Grüneisen parameter  $\gamma$  and the shear deformation parameter  $\beta$  toward the value of 1.34.

DOI: 10.1103/PhysRevB.87.085416

PACS number(s): 63.22.-m, 62.25.-g, 62.50.-p

Single-walled carbon nanotubes (SWCNTs) have significant potential in applications ranging from nanofluidics to optoelectronics, with applications already realized in composite reinforcement. Consisting of a single, rolled-up graphene sheet, they have only surface atoms and so are unusually sensitive to their environment. This sensitivity hampers investigation of many intrinsic properties of the nanotubes, in particular their response to high hydrostatic pressure.<sup>1</sup>

Raman spectroscopy has been used extensively for characterizing the structural, mechanical, and vibrational properties of SWCNTs. The Raman  $G$  band, at about  $1600\text{ cm}^{-1}$ , derives from the bulk graphite in-plane  $E_{2g}$  mode, while the low-frequency radial breathing mode (RBM) is a consequence of the tube structure. The pressure dependence of these modes carries key information about the bond anharmonicity and the mechanical strength of the curved graphene sheet. However, the Raman signal is highly resonant, and nanotube samples always contain a large number of different diameters and chiralities, denoted by the chiral indices  $(n, m)$ . The Raman spectrum is dominated by the contribution from those tubes for which the excitation photon energy or the Raman photon energy matches the electronic transition energies  $E_{ii}$ .<sup>2,3</sup> As well as shifting with pressure,<sup>4,5</sup> the electronic transition energies are also highly sensitive to the nature of the solvent or hydrostatic pressure transmitting medium (PTM) in which the nanotubes are immersed.<sup>4-6</sup> The result is that different nanotubes are in resonance for any given laser excitation energy in different solvents, and, with increasing pressure, different tubes come in and out of resonance.<sup>1</sup> As a consequence, unambiguous determination of the pressure coefficients of the Raman peaks is complicated, and, most remarkably, no clear difference between (solvent) filled and empty tubes has yet been reported.<sup>6</sup>

A large body of published work has shown that resonant Raman spectroscopy of carbon nanotubes at ambient pressure, in which both the RBM shift  $\omega_{\text{RBM}}$  and resonance energy  $E_{ii}$  are measured, gives peaks on a two-dimensional surface to which chiral indices  $(n, m)$  can be assigned. This work began with the *Kataura* plot of theoretical  $E_{ii}$  values against diameter

for all  $(n, m)$ .<sup>2</sup> More recent experimental and theoretical work refined this plot so that identification of many peaks from their  $(\omega_{\text{RBM}}, E_{ii})$  position is now unambiguous.<sup>7-11</sup> While the bulk of these studies concern unbundled nanotubes in water with surfactant, different shifts have been observed with different surfactants,<sup>7</sup> and the effect of filling open tubes with water has also been reported.<sup>11</sup>

We have reported large shifts in the  $E_{ii}$  coordinate of some  $(n, m)$  nanotubes in the form of bundles in different solvents (water, hexane, sulfuric acid) and in air.<sup>3</sup> In contrast, high pressure with water as the PTM (solvent) gives a shift, which is largely in the  $\omega_{\text{RBM}}$  coordinate.<sup>4</sup> This work demonstrated that the effects of solvent and pressure are distinct and opens the way to obtaining reliable pressure coefficients for each  $(n, m)$  not only for the RBM mode but also for the  $G$  mode. To do this, it is necessary to find a sparse region of the  $(\omega_{\text{RBM}}, E_{ii})$  map so that the  $G$ -mode resonance observed can be identified with the RBM resonance and hence with a specific tube chirality or diameter. Here we demonstrate this by obtaining the RBM and  $G$ -mode pressure coefficients for three peaks in the  $(\omega_{\text{RBM}}, E_{ii})$  map. While the results for the RBM agree well with previous literature, the  $G$ -mode data are not as expected from the current interpretation of the pressure dependence of the graphene and graphite equivalents of the  $G$  mode, an issue that we address here.

High Pressure Carbon Monoxide Process (HiPco) SWCNTs were used as purchased, without unbundling, in water as the PTM. A Ti-sapphire laser was used to perform Raman spectroscopy over the energy range  $1.48\text{ eV}$ – $1.78\text{ eV}$  at intervals of about  $10\text{ meV}$ . At each excitation energy, Raman spectra were recorded over the range  $210\text{ cm}^{-1}$ – $320\text{ cm}^{-1}$  to capture the RBM peaks and from  $1500\text{ cm}^{-1}$ – $1700\text{ cm}^{-1}$  for the  $G$ -band spectra. The RBM spectra are fitted with Lorentzian peaks (giving the positions  $\omega_{\text{RBM}}$ ), and the intensity of each peak is plotted against the laser excitation energy. The excitation energy for which the RBM intensity is maximum was taken as  $E_{ii}$  for that peak. We presented the *Kataura* plot thereby obtained, with the chiralities assigned by comparison with the results of Araujo *et al.*<sup>9,10</sup> in Ref. 4. Given the chiralities  $(n, m)$ ,

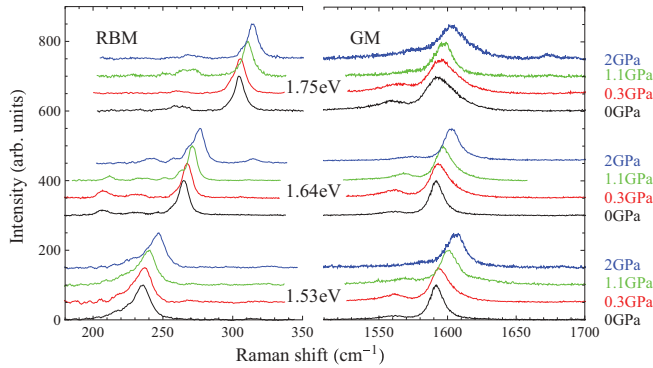


FIG. 1. (Color online) RBM and *G*-mode spectra for the excitation energies and pressures marked, offset vertically for clarity. The spectra under 1.75-eV excitation (upper group) are assigned to the (9, 1) chirality, the spectra under 1.64-eV excitation (middle group) to the (11, 0) and (10, 2) chiralities, and the spectra under 1.53 eV (lower group) to the (12, 1) and (11, 3) chiralities.

the diameters are calculated as  $d = a\pi^{-1}(n^2 + nm + m^2)^{1/2}$ , where  $a = 0.246$  nm is  $\sqrt{3}$  times the C-C bond length. At laser energies near 1.75 eV, there is a single dominant peak in the RBM spectrum (Fig. 1) that is assigned to the (9, 1) chirality ( $d = 0.747$  nm). At 1.64 eV, the peak assigned to the (11, 0) ( $d = 0.861$  nm) and (10, 2) ( $d = 0.872$  nm) chiralities dominates the spectrum, and at laser energies near 1.53 eV, it is the (12, 1) ( $d = 0.981$  nm) and (11, 3) ( $d = 1.000$  nm) peak which dominates. At most other excitation energies, there are two or more strong peaks in the RBM spectrum.

When there are multiple strong peaks in the RBM spectrum, it is expected that the associated *G*-band peak contains contributions from all of the corresponding tube chiralities or diameters. When a single RBM peak dominates the spectrum, we assume that the *G*-band peak is largely due to the same diameter tube. However, resonances with  $E_{ii}$  might occur with the outgoing Raman photon, and the effect on the Raman intensity is the same.<sup>3</sup> A resonance with the Stokes Raman photon is shifted up in energy, and a resonance with the anti-Stokes Raman photon is shifted down relative to the resonance with the excitation photon. For the RBM, these energies are too close to be resolved, and this effect merely broadens and shifts the resonance by 10–20 meV ( $1/2 \hbar\omega_{\text{RBM}}$ ). However, for the *G* mode of any given tube, this effect gives peaks about 200 meV ( $\hbar\omega_G$ ) apart in excitation energy. Consequently, any given excitation energy might be in resonance with a particular tube, giving both the RBM and *G*-mode Raman peaks of that tube, and it might also be in resonance with the Raman (Stokes) *G*-mode photon of another tube, giving the *G*-mode Raman peak but not the RBM peak for that tube. When only one RBM peak is observed, it is necessary to determine whether there might be other contributions of this sort to the *G*-mode peak. This requires considering where these resonances are on the Kataura plot.

Figure 2 shows the Kataura plot for the RBM resonances for the Hipco nanotubes bundled in water in the range of excitation energies used.<sup>4</sup> The predicted excitation and Stokes resonances for the *G* mode are also shown. For instance, we see that 1.53 eV photons, which excite the (12, 1) and (11, 3) tubes, possibly have overlapping resonance with the

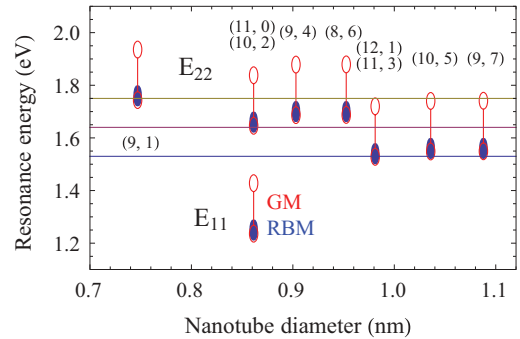


FIG. 2. (Color online) The solid ellipses represent the observed RBM resonances for Hipco nanotubes bundled in water, reported in Ref. 3. The expected resonances for the *G* mode are shown by the open ellipses; for each tube diameter the lower ellipse is for the resonance with the incident photon and the upper ellipse for the resonance with the Stokes Raman photon. The lines joining the upper and lower ellipses represent the nonzero intensity between the two peaks.

larger (10, 5) and (9, 7) tubes, but no more in the *G* band than in the RBM region. The 1.64-eV excitation is close only to the target (11, 0) and (10, 2) tubes. The 1.75-eV excitation, resonant with the (9, 1) tubes, is also close to the Stokes photon resonance of the large (10, 5) and (9, 7) tubes, but is not on the peak. We consider below what the consequences on the interpretation of our data would be if there were significant excitation of these tubes via their *G*-mode Stokes Raman photon. At lower and higher energies, there are no other tubes or  $E_{ii}$  states giving resonances that would be excited.

The pressure experiments were carried out in a diamond-anvil cell operated in the Zen configuration (using a single diamond),<sup>12</sup> which permits good control over the pressure in the range 0–2 GPa. The pressure was measured using the standard technique of ruby photoluminescence.

The dependence of both the RBM and *G*-band spectra on pressure is shown in Fig. 1 for the three excitation energies. The peak positions are plotted in Fig. 3 with linear least-squares fits to obtain the pressure coefficients. To estimate the errors due to scatter, and also because the 2 GPa points may have increased error due to the freezing of the water PTM above 1 GPa, least-squares fits to the data for the three lower pressures are also shown.

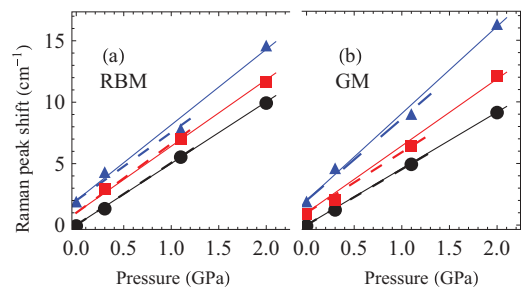


FIG. 3. (Color online) Raman shifts with pressure for (a) the RBM and (b) the *G*-mode peaks for the three excitation energies indicated in Fig. 1. The middle and upper data sets are offset for clarity by 1 cm⁻¹ and 2 cm⁻¹, respectively. The solid lines are linear least-squares fits to the whole datasets, while the dashed lines are fits to the lower three pressure points.

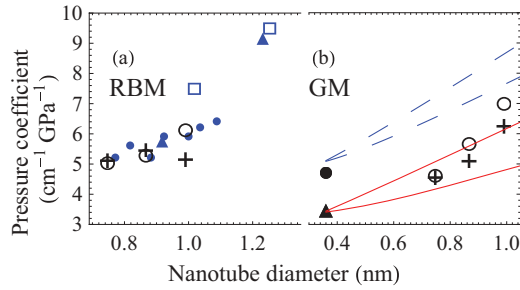


FIG. 4. (Color online) Pressure coefficients from Fig. 3 plotted against the tube diameters for the three excitation energies of Fig. 1. (a) The RBM data determined here (open circles and crosses) are compared with experimental results for bundled semiconducting tubes in ethanol/methanol (triangles; Ref. 13), unbundled semiconducting tubes in water/surfactant (small solid circles; Ref. 14), and with MD simulation results for unbundled semiconducting tubes in water (open squares; Ref. 15). (b)  $G$ -mode data determined here (open circles and crosses) are plotted together with broken lines showing the dependence on diameter expected for the  $G^+$  and  $G^-$  bands from Eq. (3) using the values for  $\gamma$  and  $\beta$  given in Ref. 19, and solid lines showing the results for the revised values discussed in the text. For comparison, the pressure coefficients of graphite (solid circle; Ref. 20) and graphene (solid triangle) [revised value from the data of Ref. 19 according to Eq. (2) with  $\varepsilon_T = 0$ ] are shown, plotted at  $d = w$ .

In Fig. 4, the pressure coefficients that we determine are plotted against the tube diameters for the fits to the lower pressure points (crosses) and for the fits that include the 2 GPa data (open circles). Literature data for the pressure coefficients of the RBM peaks of semiconducting SWCNTs are also shown. Experimental data is for the RBM of bundled tubes in an ethanol-methanol mixture from Venkateswaran *et al.*<sup>13</sup> and the RBM of unbundled tubes in  $\text{H}_2\text{O}$  with surfactant from Lebedkin *et al.*<sup>14</sup> Theoretical data is from molecular dynamics (MD) simulations of the RBM of isolated tubes in  $\text{H}_2\text{O}$  from Longhurst and Quirke.<sup>15</sup>

A striking feature of the results in Fig. 4(a) is the excellent agreement of our RBM data with the data for semiconducting debundled tubes of Lebedkin *et al.*<sup>14</sup> and for the bundled tubes of Venkateswaran *et al.*<sup>13</sup> Previously, differences in reported pressure coefficients were attributed to consequences of bundling (e.g., hexagonalization under pressure<sup>13</sup>) and to the different solvents used as PTM.<sup>1</sup> The good agreement between bundled and unbundled tubes in water and unbundled tubes in ethanol-methanol suggests that neither of these factors affects the pressure coefficients. This is a surprising but useful result.

The RBM frequency has been related to the  $G$ -band frequency by Venkateswaran *et al.*<sup>13</sup> using a continuous elastic medium approximation and by Gerber *et al.*<sup>16</sup> using a simple ball-and-spring model. In both analyses, good agreement is obtained with the empirical dependence of  $\omega_{\text{RBM}}$  on diameter. Both imply a small RBM pressure coefficient of about  $0.8d^{-1} \text{ cm}^{-1} \text{ GPa}^{-1}$  where the tube diameter  $d$  is in nanometers [before correction for the thick-wall effect, see Eq. (1) below], which is very much less than the values observed experimentally. The MD simulations of Longhurst and Quirke<sup>15</sup> explain this in terms of the interaction between the (unbundled) nanotube and its environment by considering a nanotube surrounded by water molecules at high pressure.

The van der Waals interaction between the nanotube and the first shell of water molecules provides only a small correction to the ambient-pressure RBM frequency, but the increase in the force constant of this interaction with pressure gives the bulk of the RBM pressure coefficient. This is a greater effect for low RBM frequencies (large tubes) than for high RBM frequencies (small tubes), giving the dependence of the pressure coefficient on the diameter seen in Fig. 3(a). The good agreement of the data for bundled tubes in water, unbundled tubes in water and surfactant, and bundled tubes in ethanol-methanol suggests that the increase in the force constant of the interaction between the nanotube and its environment is similar in all cases. It would seem that the same RBM pressure coefficient (within experimental error) is obtained by the stiffening of the internanotube van der Waals interaction in nanotube bundles as by the stiffening of the water (or surfactant) van der Waals interaction with unbundled tubes.

The  $G$ -band pressure coefficients in Fig. 4(b) are remarkably low—in this low-pressure range, values up to 8 or  $10 \text{ cm}^{-1}\text{GPa}^{-1}$  have commonly been reported<sup>1</sup>—and exhibit a strong dependence on tube diameter. The dependence on diameter might be understood by considering the nanotube as a thick-walled closed tube under external pressure,  $P$ .<sup>17,18</sup> For an outside diameter of  $d + w$  and an inside diameter of  $d - w$  with  $d > w$ , the axial and tangential stresses are greater than the pressure  $P$ ,

$$\sigma_L = \frac{(d+w)^2}{4dw}P, \quad \sigma_T = \frac{d+w}{2w}P. \quad (1)$$

These are unequal, so to predict the pressure coefficient we require both the hydrostatic and the shear deformation parameters (mode Grüneisen parameters)  $\gamma$  and  $\beta$ . These are available from the experimental data of Mohiuddin *et al.*,<sup>19</sup> who studied the Raman  $G$ -band in graphene as a function of uniaxial strain, obtained by flexure of a beam to which a graphene flake adhered. Under uniaxial strain, the  $G$  band splits into two components,  $G^+$  and  $G^-$ . Dropping unnecessary notation and combining their Eq. (3) with their experimental results, they gave

$$\begin{aligned} \omega_{\varepsilon_L}^{G^\pm} &= \frac{\partial \omega^{G^\pm}}{\partial \varepsilon_L} = -2125 \mp 1045 \text{ cm}^{-1} \\ &= -\omega_0^G \gamma (\varepsilon_L + \varepsilon_T) \pm 1/2 \omega_0^G \beta (\varepsilon_L - \varepsilon_T), \end{aligned} \quad (2)$$

where  $\varepsilon_L$  is the longitudinal strain imposed on the graphene flake by the curvature of the substrate beam. They used the Poisson ratio  $\nu = 0.33$  of the substrate to obtain the transverse strain  $\varepsilon_T = -\nu\varepsilon_L$ , and, using the experimental value of  $\omega_0 = 1590 \text{ cm}^{-1}$  for the  $G$ -band frequency at ambient pressure, they obtained the  $G$ -mode parameters as  $\gamma = 1.99$  and  $\beta = 0.99$ . The hydrostatic strain coefficient of graphene under hydrostatic pressure  $P$  is  $\omega_{\varepsilon}^{G^\pm} = 2\omega_0\gamma = -6340 \text{ cm}^{-1}$ , which, with  $(s_{11} + s_{12})^{-1} = 1250 \text{ GPa}$ , corresponds to  $\omega_P^{G^\pm} = 5.07 \text{ cm}^{-1} \text{ GPa}^{-1}$  in good agreement with experimental values for graphite.<sup>20</sup> However, using  $\varepsilon_T = -\nu\varepsilon_L$  for the transverse strain is incorrect. For a thin beam in flexure, as the tensile part above the neutral plane tries to contract laterally and the compressive part below tries to expand, anticlastic curvature develops. Only if the anticlastic curvature is completely unconstrained is  $\varepsilon_T = -\nu\varepsilon_L$ . Otherwise, if the anticlastic

curvature is constrained by the beam aspect ratio<sup>21</sup> or by the loading contacts, there may be little or no transverse strain, i.e., this might be better treated as a plane strain problem.<sup>22</sup> Taking this limiting case and putting  $\varepsilon_T = 0$  in Eq. (2) gives  $\gamma = 1.34$  and  $\beta = 1.31$ , or within experimental accuracy,  $\gamma \sim \beta \sim 4/3$ . Then the predicted pressure coefficient for graphene and graphite from the experimental data of Ref. 19 becomes  $3.40 \text{ cm}^{-1} \text{ GPa}^{-1}$ .

For the nanotube, using Eq. (1) for the axial and tangential stresses under a pressure  $P$  and taking  $\nu = 0.13 = -s_{12}/s_{11}$ ,  $s_{11} + s_{12} = 1/1250 \text{ GPa}$  as in Ref. 19, the strains and the pressure coefficients of the  $G^\pm$  bands are given by

$$\begin{aligned} \varepsilon_L &= s_{11}\sigma_L + s_{12}\sigma_T, & \varepsilon_T &= s_{12}\sigma_L + s_{11}\sigma_T \\ \varepsilon_H &= \varepsilon_L + \varepsilon_T, & \varepsilon_S &= \varepsilon_L - \varepsilon_T \\ \omega_P^{G^\pm} &= \omega_0\gamma\varepsilon_H \mp 1/2\omega_0\beta\varepsilon_S. \end{aligned} \quad (3)$$

These curves, plotted in Fig. 4(b) against  $d$  for  $w = 0.36 \text{ nm}$  for the values of  $\gamma = 1.99$  and  $\beta = 0.99$ <sup>19</sup> (broken curves), do not agree with the experimental data. Plotting them for the revised values of  $\gamma = 1.34$  and  $\beta = 1.31$  (solid curves) reveals much better agreement with the data, within experimental uncertainty. In these fits, we have not taken into account the effect of the wall curvature on the Raman frequencies or pressure coefficients.<sup>23</sup>

Here we should consider also the possible consequence of Fig. 2, that is, that there may be some contribution to the  $G$  band of the nanotube diameters that we ruled out previously. Clearly, if the  $G$  band was always given equally by all nanotube diameters, its pressure coefficient would not vary with excitation energy. Since it does, the observed values must be attributed to the different tube diameters. However, it is possible that the pressure coefficient we attribute to the (12, 1) and (11, 3) tubes ( $d = 0.98 \text{ nm}$ ) with 1.53-eV excitation comes partly from the tubes with diameters up to 1.1 nm. This would improve the agreement in Fig. 4(b) between the observed and calculated values.

These results are surprising. With the maximum revision for plane strain of the result of the uniaxial experiment of Mohiuddin *et al.*,<sup>19</sup> we have good agreement between their data and the data for nanotubes under high pressure. On the other hand, these results are in sharp disagreement with data for graphene and graphite under high pressure, where much higher pressure coefficients are reported. Initial experiments on graphene under hydrostatic pressure<sup>24</sup> gave  $G$ -mode peak shifts as a function of strain/pressure that were consistent with density functional theory (DFT) calculations<sup>24</sup> and simple mechanical models assuming that the Raman peak shifts are due entirely to the bond stiffening when the C-C bond length is decreased. However, more recent experimental results<sup>25</sup> showed the graphene  $G$ -mode pressure coefficient varying from  $8\text{--}11 \text{ cm}^{-1} \text{ GPa}^{-1}$  according to the choice of PTM, as observed in nanotubes.

If a significant part of the  $G$ -mode pressure coefficient derives from interaction with the environment, it is noteworthy that the uniaxial stress experiment on graphene and nanotubes under pressure (whether bundled or unbundled) have condensed matter (solid or liquid) in contact with only one side of the graphene sheet. In contrast, graphene under pressure and graphite both have condensed matter (solid or liquid) in contact with both sides of each graphene sheet. Without speculating on the origin of the environmental effect, there is scope for it being twice as large in this case. This requires that a significant part of the graphite pressure coefficient is due to interactions between the graphene sheets (each sheet serving as part of the environment of its neighbors).

This interpretation also predicts that open tubes that fill with PTM will display a higher pressure coefficient than expected from the data for closed tubes (but independent of diameter). This might explain why no clear difference has been reported between closed tubes with pressure coefficients raised by the thick-wall effect [Eq. (1)] and open tubes.<sup>6</sup>

In pressure experiments on double-walled nanotubes,<sup>26,27</sup> the inner tube has condensed matter on only one side, while the outer tube has it on both sides. The pressure coefficients of the inner tubes ( $3.3\text{--}5.1 \text{ cm}^{-1} \text{ GPa}^{-1}$ ) are consistently much lower than those of the outer tubes ( $5.8\text{--}8.6 \text{ cm}^{-1} \text{ GPa}^{-1}$ ).<sup>26</sup> These data were interpreted in terms of the intertube pressure,<sup>25</sup> but the data are also consistent with the environmental effect suggested here.

The data reported here utilize tunable laser excitation to obtain the first reliable pressure coefficients for both the RBM and  $G$ -mode Raman peaks of individual SWCNTs that might be assigned to chirality and diameter. Experimentally, it is clearly urgent to find the  $G$ -mode pressure coefficients for nanotubes for a larger range of diameters, in different solvents, and for open tubes as well as closed. The results for the RBM peaks show that the increase in the force constant of the interaction between the nanotube and its immediate surroundings at high pressure occurs in a similar manner for tubes surrounded by other nanotubes, surfactant, or solvent. The results for the  $G$  band are unexpected and have prompted a reappraisal of the available data for the deformation potentials of graphene. Theoretically, they suggest the desirability of calculation *ab initio* of graphene, when the  $\pi$  orbitals are compressed by an adjacent graphite layer or PTM on one side and on both sides. This study represents a major step forward to achieving a unified understanding of the characteristics of graphene-based structures under stress and gives clear indications as to what further studies are necessary to complete this understanding.

We acknowledge financial support from the Engineering and Physical Sciences Research Council. I.H. acknowledges funding from the Royal Academy of Engineering and the European Union (FP7 MC-CIG).

\*d.dunstan@qmul.ac.uk

<sup>1</sup>D. J. Dunstan and A. J. Ghandour, *High Press. Res.* **29**, 548 (2009).<sup>2</sup>H. Kataura, Y. Kumazawa, Y. Maniwa, I. Umezū, S. Suzuki, Y. Ohtsuka, and Y. Achiba, *Synth. Met.* **103**, 2555 (1999).

- <sup>3</sup>C. Fantini, A. Jorio, M. Souza, M. S. Strano, M. S. Dresselhaus, and M. A. Pimenta, *Phys. Rev. Lett.* **93**, 147406 (2004).
- <sup>4</sup>A. J. Ghandour, A. Sapelkin, I. Hernandez, D. J. Dunstan, I. F. Crowe, and M. P. Halsall, *High Pressure Research* **32**, 67 (2012).
- <sup>5</sup>R. S. Deacon, K.-C. Chuang, J. Doig, I. B. Mortimer, and R. J. Nicholas, *Phys. Rev. B* **74**, 201402 (2006).
- <sup>6</sup>A. Merlen, N. Bendiab, P. Toulemonde, A. Aouizerat, A. San Miguel, J. L. Sauvajol, G. Montagnac, H. Cardon, and P. Petit, *Phys. Rev. B* **72**, 035409 (2005).
- <sup>7</sup>J. Maultzsch, H. Telg, S. Reich, and C. Thomsen, *Phys. Rev. B* **72**, 205438 (2005).
- <sup>8</sup>H. Telg, J. Maultzsch, S. Reich, and C. Thomsen, *Phys. Status Solidi B* **244**, 4006 (2007).
- <sup>9</sup>P. T. Araujo, A. Jorio, M. S. Dresselhaus, K. Sato, and R. Saito, *Phys. Rev. Lett.* **103**, 146802 (2009).
- <sup>10</sup>P. T. Araujo, P. B. C. Presce, M. S. Dresselhaus, K. Sato, R. Saito, and A. Jorio, *Physica E* **42**, 1251 (2010).
- <sup>11</sup>S. Cambré, B. Schoeters, S. Luyckx, E. Goovaerts, and W. Wenseleers, *Phys. Rev. Lett.* **104**, 207401 (2010).
- <sup>12</sup>N. W. A. van Uden and D. J. Dunstan, *Rev. Sci. Instrum.* **71**, 4174 (2000).
- <sup>13</sup>U. D. Venkateswaran, D. L. Masica, G. U. Sumanasekara, C. A. Furtado, U. J. Kim, and P. C. Eklund, *Phys. Rev. B* **68**, 241406 (2003).
- <sup>14</sup>S. Lebedkin, K. Arnold, O. Kiowski, F. Hennrich, and M. M. Kappes, *Phys. Rev. B* **73**, 094109 (2006).
- <sup>15</sup>M. J. Longhurst and N. Quirke, *Phys. Rev. Lett.* **98**, 145503 (2007).
- <sup>16</sup>I. C. Gerber, P. Puech, A. Gannouni, and W. Bacsa, *Phys. Rev. B* **79**, 075423 (2009).
- <sup>17</sup>J. Sandler, M. S. P. Shaffer, A. H. Windle, M. P. Halsall, M. A. Montes-Morán, C. A. Cooper, and R. J. Young, *Phys. Rev. B* **67**, 035417 (2003).
- <sup>18</sup>J. A. Elliott, J. K. W. Sandler, A. H. Windle, R. J. Young, and M. S. P. Shaffer, *Phys. Rev. Lett.* **92**, 095501 (2004).
- <sup>19</sup>T. M. G. Mohiuddin, A. Lombardo, R. R. Nair, A. Bonetti, G. Savini, R. Jalil, N. Bonini, D. M. Basko, C. Galiotis, N. Marzari, K. S. Novoselov, A. K. Geim, and A. C. Ferrari, *Phys. Rev. B* **79**, 205433 (2009).
- <sup>20</sup>M. Hanfland, H. Beister, and K. Syassen, *Phys. Rev. B* **39**, 12598 (1989).
- <sup>21</sup>W. C. Young and R. G. Budynas, *Roark's Formulas for Stress and Strain*, 7th ed. (McGraw-Hill, New York, 2002), Sec. 8.11.
- <sup>22</sup>S. P. Timoshenko and J. N. Goodier, *Theory of Elasticity*, 3rd ed. (McGraw-Hill, New York, 1970).
- <sup>23</sup>A. L. Aguiar, R. B. Capaz, A. G. Souza Filho, and A. San-Miguel, *J. Phys. Chem. C* **116**, 22637 (2012).
- <sup>24</sup>J. E. Proctor, E. Gregoryanz, K. S. Novoselov, M. Lotya, J. N. Coleman, and M. P. Halsall, *Phys. Rev. B* **80**, 073408 (2009).
- <sup>25</sup>J. Nicolle, D. Machon, P. Poncharal, O. Pierre-Louis, and A. San-Miguel, *Nano Lett.* **11**, 3564 (2011).
- <sup>26</sup>P. Puech, H. Hubel, D. J. Dunstan, R. R. Bacsa, C. Laurent, and W. S. Bacsa, *Phys. Rev. Lett.* **93**, 095506 (2004).
- <sup>27</sup>P. Puech, E. Flahaut, A. Sapelkin, H. Hubel, D. J. Dunstan, G. Landa, and W. S. Bacsa, *Phys. Rev. B* **73**, 233408 (2006).